SCIENCE CHINA
Chemistry

•ARTICLES•
SPECIAL ISSUE: Celebrating the 60th Anniversary of the University of Science and Technology of China

September 2018 Vol.61 No.9: 1187–1196
https://doi.org/10.1007/s11426-018-9273-1

Single atom accelerates ammonia photosynthesis

Pengcheng Huang[1], Wei Liu[2], Zhihai He[1], Chong Xiao[1*], Tao Yao[2], Youming Zou[3], Chengming Wang[1], Zeming Qi[2], Wei Tong[3], Bicai Pan[1], Shiqiang Wei[2] & Yi Xie[1*]

[1]*Hefei National Laboratory for Physical Sciences at the Microscale, CAS Center for Excellence in Nanoscience, iCHEM, University of Science and Technology of China, Hefei 230026, China;*
[2]*National Synchrotron Radiation Laboratory, University of Science and Technology of China. Hefei 230029, China;*
[3]*High Magnetic Field Laboratory, Chinese Academy of Sciences, Hefei 230031, China*

Received April 22, 2018; accepted April 24, 2018; published online June 15, 2018

Atomically dispersed metal has gained much attention because of the new opportunities they offer in catalysis. However, it is still crucial to understand the mechanism of single-atom catalysis at molecular level for expanding them to other more difficult catalytic reactions, such as ammonia synthesis from nitrogen. In fact, developing ammonia synthesis under ambient conditions to overcome the high energy consumption in well-established Haber-Bosch process has fascinated scientists for many years. Herein, we demonstrate that single Cu atom yields facile valence-electron isolation from the conjugated π electron cloud of p-CN. Electron spin resonance measurements reveal that these isolated valence electrons can be easily excited to generate free electrons under photo-illumination, thus inducing high efficient photo-induced ammonia synthesis under ambient conditions. The NH_3 producing rate of copper modified carbon nitride (Cu-CN) reached 186 μmol g^{-1} h^{-1} under visible light irradiation with the quantum efficiency achieved 1.01% at 420 nm monochromatic light. This finding surely offers a model to open up a new vista for the ammonia synthesis at gentle conditions. The introduction of single atom to isolate the valence electron also represents a new paradigm for many other photocatalytic reactions, since the most photoinduced processes have been successfully exploited sharing the same origin.

single atom, photocatalytic, ammonia synthesis

Citation: Huang P, Liu W, He Z, Xiao C, Yao T, Zou Y, Wang C, Qi Z, Tong W, Pan B, Wei S, Xie Y. Single atom accelerates ammonia photosynthesis. *Sci China Chem*, 2018, 61: 1187–1196, https://doi.org/10.1007/s11426-018-9273-1

1 Introduction

Nitrogen is an essential nutrient for all living organisms, and nitrogen fertilizer is one of the important guarantees to meet global food requirements. However, its molecular form, though it composes nearly 80% of the atmosphere, is difficult to utilize due to its strong nonpolar N≡N covalent triple bond, which inhibits dissociation [1]. Therefore, nitrogen fixation before intake by organisms is a required transformation, but this only occurs in nature within microbial organisms containing enzymes called nitrogenases [2]. Although the N_2 can be converted to NH_3 artificially by the well-established Haber-Bosch process, this process is accomplished under drastic conditions, such as high temperature (300–500 °C) and pressure (150–250 atmospheres), consuming more than 1% of the world's energy supply and producing a large amount of greenhouse gas emissions [3]. In view of the fossil fuel shortage and global climate change, achieving nitrogen fixation under mild conditions to overcome the high energy consumption of the Haber-Bosch process is a crucial subject in chemistry [4–10] and has fascinated scientists for many years. In fact, in 1977, Schrauzer and Guth [11] reported that N_2 can be reduced to NH_3 under UV-light irradiation by iron-doped TiO_2. Though

*Corresponding authors (email: cxiao@ustc.edu.cn; yxie@ustc.edu.cn)

numerous works have been devoted to this topic, achieving a high conversion efficiency remains a challenge [12]. It is well known that the complex six-electron reduction process in the conversion of N_2 to ammonia typically hampers N_2 cleavage on the photocatalyst [13]. Therefore, the design of a new photocatalyst that has sufficient photoexcited electrons to participate in the reduction process is a key requirement for photocatalytic ammonia synthesis, however, this remains urgent and challenging.

Very recently, polymeric carbon nitride (p-CN) has emerged as a potential polymeric photocatalyst for various relevant chemical reactions, including water splitting, CO_2 reduction, phenol synthesis from benzene, and the selective oxidation of aromatic alcohols, due to its suitable electronic band structure, good chemical stability, molecular tenability and low cost [14–17]. However, the photocatalytic activity of pristine p-CN is quite low due to the intrinsic drawbacks derived from the conjugated quasi two dimensional π system. The incomplete heptazine cyclization and impurities can be catalytically relevant and may, in fact, is some of the catalytically active "defects" cited in the literature, just as Wang *et al.* [18] proposed "surface terminations and defects seem to be the real active sites". To elucidate the identities of the catalytically relevant surface terminations of carbon nitride by employing heptazine-based molecules as model catalyst. The methodology employed to circumvent complication from surface heterogeneity and structural ambiguity in heterogeneous catalysis research is particularly suitable for studying melon-like materials, because of its amorphous nature and lack of solubility, could only be structurally resolved nearly two centuries after its discovery [19–23]. Inspected from the X-ray photoelectron spectroscopy (XPS) results (Figure S1(a), Supporting Information online) of nitrogen element in our catalyst, in which the N existing form consists of scaffold N atoms (N–$(C)_3$), edge N atoms (C–N=C) as well as termination N atoms (C–N–H_x). For the scaffold N atoms, the lone pair electrons are confined in the conjugated electron cloud as we know, while for the edge N-atoms of the triazine or heptazine ring, which make up a large proportion, two of the valence electrons are utilized to bond adjacent C atoms, left another valence electron becoming the π electron, thus generating a pair of lone electrons stretching outside the ring (as seen in Figure S1(c, d)). Meanwhile, as a typical characteristic of polymeric photocatalysts, the lone-pair electrons originated from the nitrogen atoms with a sp^2 hybridized structure in p-CN allow these N atoms to act as donors to interact with exogenous matter. Thus the N/C-coordinating framework formed by the unique triazine and heptazine structure facilitates the binding or intercalation of exotic atoms into the matrix of p-CN, such as protons [24]. For example, it has been reported that the introduction of dangling hydrogen bonds onto p-CN ultrathin nanosheets produced obvious room-temperature ferromagnetic behavior [25]. Apart from the main body of the hydrogen content derive from the incomplete terminal groups, the additional loading of the hydrogen is attributed to the protonation of these imino or amino groups, including the protonated edge N atoms. After carefully scrutinizing this phenomenon, we determined that the H atoms were bound to the N atoms through the lone-pair electrons, which undoubtedly implies that the manipulation of lone-pair electrons should be an effective strategy to interact with extraneous matter. Generally speaking, to promote the photocatalytic activity of p-CN, the preferred approach is to generate more excitons which are located within each triazine or heptazine unit of the polymer [26,27]. Although many strategies, such as copolymerization, doping and hybridization [28–30], have been developed to achieve this objective, the activated conjugated electrons are still constrained in the π bond. Inspired by other excellent work [31,32], through the hetero-homogeneous co-catalysts could we improve the interfacial charge transfer and contribute to the relevant catalytic reaction process.

During the development of advanced catalysts, single metal atoms anchored on substrates have recently attracted increasing research attention [33–36] due to their unique catalytic properties and maximized atom efficiency to provide low-cost systems. However, it is still of great importance to understand the mechanisms of single-atom catalysis at the molecular level for the rational design of superior-performing catalysts. Most empty orbitals become occupied when ionic single atoms, such as transition metal ions, are introduced, which enables the ions to easily bind to the polymer through interaction with the lone-pair electrons. Therefore, it is reasonable to assume that manipulating the lone-pair electrons with single metal atoms is desirable.

Herein, based on the theory and experiments above, we demonstrate the manipulation of lone-pair electrons by incorporating scarce single copper atoms onto the defects of carbon nitride ultrathin nanosheets to realize the high-performance photoilluminated synthesis of ammonia under ambient conditions for the first time. The X-ray absorption fine structure (XAFS) results demonstrated a novel threefold coordination of Cu atoms, which resulted in the single valence electron of coordinated N atom delocalized or even isolated from the π conjugated electron cloud due to the theoretical calculations. The isolated single electron is much easier activated for involvement in the relevant photocatalytic reaction, which results in a significant improvement of the activity in ammonia synthesis, nearly 8 times compared with that of pristine p-CN. The photocatalytic synthesis of ammonia by Cu-CN reached 186 μmol g^{-1} h^{-1} under visible-light irradiation, with a quantum efficiency of 1.01% under 420 nm monochromatic light. This new strategy of manipulating lone-pair electrons of defect atoms to activate the single π electron firstly reported here undoubtedly re-

presents a new paradigm not only for ammonia synthesis but also for other photocatalytic reactions under mild conditions.

2 Experimental

2.1 Synthesis of p-CN and Cu-CN

The p-CN was synthesized by thermal polymerization of fully mixed 1 g of dicyandiamide powder and 5 g ammonium chloride in a covered crucible at 550 °C for 4 h at a ramp rate of 3 °C min^{-1}. The resulting materials were characterized as polymeric carbon nitride nanosheets [29]. The Cu-CN was prepared by dispersing 50 mg of the as-prepared p-CN nanosheets into 15 mL $CuCl_2$ (1 mM) aqueous solution and keeping stirring at 60 °C for 4 h. The resulting product was centrifuged at 14000 r min^{-1} for 3 min and washed with distilled water and ethanol for several times then dried in vacuum at 60 °C overnight, followed by annealing at 125 °C for 1 h in N_2 atmosphere. Sample with 0.080 wt% Cu loading was labelled as Cu-CN, which was measured by inductively coupled plasma-atomic emission spectrometry.

2.2 Characterization

The samples were characterized by X-ray powder diffraction (XRD) by Phillips X'Pert Pro Super diffractometer (USA) equipped with graphite-monochromatized Cu-Kα radiation (λ=1.54178 Å). Transmission electron microscopy (TEM) images were obtained using H-7650 (Hitachi, Japan) operated at an acceleration voltage of 100 kV. XPS measurements were performed on a VG ESCALAB MK II X-ray photoelectron spectrometer (UK) with an exciting source of Mg Kα=1253.6 eV. UV-Vis-NIR absorption spectra measured for powder samples were on a Shimadzu Solid 3700 (Japan). UV-Vis diffuse reflectance spectra of samples were obtained using a Perkin Elmer Lambda 950 UV-Vis-NIR spectrometer (USA). Electron Spin Resonance (ESR) signals were recorded on a Bruker EMX plus model spectrometer (Germany) operating at X-band (9.4 GHz) from 2 to 80 K. The photoluminescence (PL) spectrum was obtained by JY Fluorolog-3-Tou fluorescence spectrometer (USA) equipped with an integrating sphere and the excitation wavelength was 365 nm. The transient photocurrent was measured by CHI 760E electrochemistry work station (Japan). The high-angle annular dark-field scanning transmission electron microscopy (HAADF-STEM) characterization was performed on a JEOL JEM-ARF200F TEM/STEM with a spherical aberration corrector (Japan). The loadings of Cu were measured on inductively coupled plasma-atomic emission spectrometer (ICP-AES) on an Optima 7300 DV (Perkin-Elmer Corporation, USA). The XAFS spectra were collected at the BL14W1 beamline of Shanghai synchrotron radiation facility (SSRF, China). The storage ring of the SSRF was operated at 3.5 GeV with the electron current of 200 mA.

2.3 Photocatalytic dinitrogen fixation activity measurements

The photocatalytic N_2 fixation experiments were conducted in a 50 mL quartz reaction cell with an external cooling water jacket at ambient temperature and atmospheric pressure. A 300 W Xe lamp through an UVIR cut-off filter (780 nm>λ>420 nm) was used as the simulated Sunlight source. In a typical experiment, 50 mg of photocatalyst powder was dispersed in 50 mL of aqueous solution containing 20 vol% ethanol. N_2 (purity≥99.999%) was bubbled through this solution for 1 h in dark before radiation to establish an adsorption-desorption balance and saturate the solution with N_2. Then the reactor was sealed and irradiated with visible light (λ>420 nm). During light irradiation, approximately 3 mL of the suspension was extracted through a syringer from the reaction cell at given intervals for subsequent NH_4^+ concentration analysis.

NH_4^+ concentration analysis was conducted using Nessler's reagent method. First, 3 mL of the suspension was filtered through a 0.22 μm membrane filter and placed in a 25 mL sample tube and diluted with non-ammonia water into the specific scale line. Then, 0.5 mL of the potassium sodium tatrate solution was added to the sample tube. After blending and standing for several minutes, 0.5 mL of Nessler's reagent was added to the same sample tube and fully mixed. Also left standing for several minutes for full color processing. Finally, the concentration of NH_4^+ was tested using an UV-Vis-NIR spectrophotometer (Lambda 950, USA) at λ=425 nm.

2.4 ESR measurement

ESR spectra were performed by Bruker EMX plus model spectrometer operating at X-band (9.4 GHz). The sample was dispersed in ethanol at 1 mg mL^{-1} before, containing 20 vol% glycerol. The tube was pre-cooled in liquid nitrogen before set into the spectrometer. The light irradiation was achieved through an optical fiber onto the tube chamber and signal was also recorded at different set temperature. After the irradiation we still recorded the signal to investigate the origin of enhanced difference.

2.5 *In-situ* FTIR measurement

In-situ diffuse Fourier transform infrared (FTIR) spectra were performed by Bruker 66V FTIR spectrometer (Germany) with a specific reaction cell [37]. The groove in the center of the specific loading platform was pre-filled with the powder of KBr and smoothed out. Then two nets were set between the substrate and sample before the placement of the

p-CN and Cu-CN powders. A little amount of water was necessary for the generation of proton and pre-adsorbed on the surface by moisting the surface of the sample before the molecular dinitrogen was pumped in. The pumping process took around 5 min to fully expel the containing air and built a N_2 atmosphere. At last, the intake valve and outlet valve were closed to construct a closed chamber and light was turned on irradiating through an optical fiber and IR signal was *in situ* recorded through a MCT detector along with the reaction.

2.6 DFT calculation

All calculations are performed using spin-polarized density functional theory methods as implemented in the Vienna *ab initio* simulation package (VASP) [38], where the interaction between ions and valence electrons is described with the projector augmented wave (PAW) potentials [39–41], and the exchange-correlation between electrons is described by the generalized gradient approximation (GGA) in the Perdew-Burke-Ernzerhof (PBE) form [42]. The kinetic energy cutoff for the plane-wave basis set is 500 eV. The periodic boundary conditions are applied and a vacuum region of 15 Å is used to avoid the interaction between the sheet and its images. In addition, the 3×3×1 *k* points within the gamma centered Monkhorst-Pack scheme is used to sample the Brillouin zone for all the structures [43]. The lattice parameters and the atomic coordinates are fully relaxed until the forces on each atom is less than 0.02 eV $Å^{-1}$. For the adsorption of nitrogen, the DFT-D_2 method [44,45] is used for the vdW corrections.

The adsorption energy of N_2 is defined as:

$$E_{ad} = E_{layer+N_2} - E_{layer} - E_{N_2}$$

where $E_{layer+N_2}$ and E_{layer} are the total energy of CN layer with and without the N_2 molecule, respectively, E_{N_2} is the total energy of an N_2 molecule.

The difference of Gibbs energy is calculated by:

$$\Delta G = E_{ad} + \Delta E_{ZPE} - T\Delta S + \Delta H$$

where E_{ad} is the adsorption energy at 0 K, ΔE_{ZPE} is the difference in zero-point energy, ΔS and ΔH are entropy and enthalpy contribution from 0 to 298.15 K for reaction energy.

3 Results and discussion

Ultrathin polymeric carbon nitride (p-CN) nanosheets were prepared through the gas-template thermal polymerization of a mixture of dicyandiamide and ammonium chloride in a covered alumina crucible. Cu-CN was manufactured via impregnation of the $CuCl_2$ solution in the as-prepared p-CN powders at relatively low temperature, followed by post-annealing. Figure 1(a) shows the X-ray diffraction (XRD) patterns of the as-obtained samples, which show the stacking (002) and in-plane (100) periodicties at 27.6° and 12.8°, respectively, are in well agreement with the previously reported patterns for p-CN. No peaks corresponding to copper-based compound was detected in the Cu-CN pattern, indicating its high purity and no structure damages happened. In addition, the broad XRD pattern and unobvious lattice fringes indicate the poor crystallinity of as-obtained samples, which endows the defect-rich nature. A multi-layer stacked planar structure was observed at the edge of the nanosheets in the HRTEM image (as shown in Figure 1(b)), demonstrating the quasi two-dimensional characteristic. Meanwhile, the inductively coupled plasma-atomic emission spectroscopy (ICP-AES) results revealed that the Cu loading in Cu-CN was confirmed and relatively low around 0.089 wt% (Table S1, Supporting Information online). The state of Cu in the prepared catalyst was analysed by the XPS of Cu 2p spectrum (Figure S1(b)). Binding energy peaks were obtained for Cu $2p_{3/2}$ and Cu $2p_{1/2}$ at 932.2 and 952.2 eV, respectively, typical values for Cu^{2+}. There were also two shakeup satellite peaks acquired at 942 and 962 eV, which are the characteristic of Cu^{II} with the d^9 transition metal electron configuration. In this case, we performed the high-angle annular dark-field scanning transmission electron microscopy (HAADF-STEM) to further explore the visual distribution of Cu atoms on p-CN. The selected area in Figure 1(b) was amplified and shown in Figure 1(c), in which the moderately dispersed brighter spots (highlighted by red dotted line circles) on the plane, representing the Cu atoms, were uniformly isolated embedded on CN.

As we obtained the existence and visual dispersion of the Cu atoms on the polymeric carbon nitride, the specific chemical environment of Cu atoms was still unclear. To investigate the particular local structure of the Cu atoms incorporated in the CN substrate, we utilized the synchrotron-radiation X-ray absorption fine structure (srXAFS) spectra of Cu-CN at the Cu K-edge, which is one of the most powerful techniques to probe the local electronic and geometrical structures adjacent to the selected element. Figure S2(a) shows the experimental Cu K-edge XANES spectra of Cu-CN and Cu foil. Figure 1(d) shows the Fourier transforms (FT) of the Cu K-edge XAFS oscillation of the as-prepared Cu-CN, compared with standard Cu foil. The FT-XAFS spectra of Cu-CN show a single sharp peak with a total Gaussian distribution at approximately 1.5 Å, which is a presentative value needing further calibration and obviously less than that of standard Cu foil. The absence of a Cu–Cu bond further confirms the isolated single-atom configuration of Cu in Cu-CN. Furthermore, to determine the quantitative chemical configuration around Cu atoms in the as-obtained Cu-CN, a least-squares curve simulation fitting was conducted in the r-space using the IFEFFIT software [46]. Figures 1(e) and S2(b) show the simulation fit curves of Cu-CN,

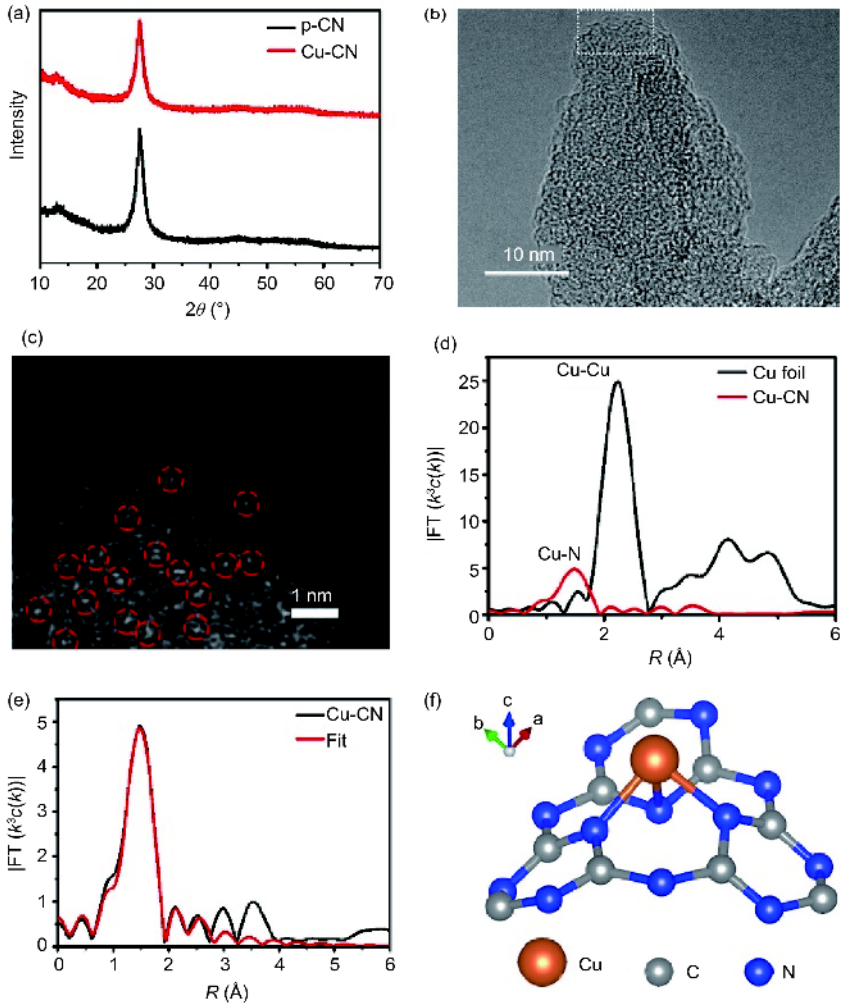

Figure 1 (a) XRD patterns for p-CN and Cu-CN. (b) HRTEM and (c) HAADF-STEM image of Cu-CN. (d) FT-EXAFS curves of Cu foil and Cu-CN. (e) FT-EXAFS curves of the experimental data and the fit of Cu-CN. (f) Proposed configuration of Cu-CN in a T-defect (color online).

which are perfectly reproduced and in well agreement with the experimental FT-XAFS curves, so do the Cu foil in Figure S2(c, d). According to the fit parameters (as shown in Table S2) the bond was fitted to be Cu-N, the coordination number was 3 and the bond length was determined to be 1.95 Å with a proper calibration. The XAFS results gave us novel information on the coordination of incorporated Cu atoms in the CN network, after cautiously searching the probable sites in representative triazine and heptazine model for triple coordination situation, we found numerous planar defects could be possible in such complex polymer, among which there were two regular possible proposed configurations stacked by the constructive repeating units in p-CN, e.g., a triangle defect (T-defect) usually formed by the edge N atoms of the triazine patch and a heptazine defect (H-defect) commonly built by the edge N atoms of the heptazine patch as well [47], which could both provide donor N atoms to meet the actual need. Therefore, based on the XAFS experimental and fitting results, we performed the density functional theory (DFT) calculation to determine the preferred local defect anchor site for Cu in the p-CN. As shown in Table S3, illustrating as many adsorbing sites as we can, these potential defect anchor sites in the T-defect, H-defect, where Cu atoms were bound to donor N atoms with constrained bond length specifically, were simulated and the adsorption energy was calculated. The optimized calculation results show that the most appropriate structure would be in T-defect, where the Cu atoms are on the top of the triangle voids in CN network and without the interference of other atoms, the adsorption energy of single Cu atom in T-defect is the lowest among all anchor sites in these defect types simulation, demonstrating the most approximate configuration of Cu single atoms in our prepared catalyst. The other anchor sites, either the bond length is irregular or the closest neighbour atoms are more than three which has no match to the XAFS fit results. As for the rest types of adsorption sites, such as side chain or edge area of the conjugated rings, may attract a little Cu atoms through relatively lower electrostatic adsorption, and the Cu atoms would be easily washed away during the washing and high-speed centrifugation process. In

this case the most stable existence formation of Cu was fitted to coordinate with three N atoms. Based on the ICP-AES results, XPS spectrum, HAADF-STEM images, XAFS measurement and DFT calculations above, it can be concluded that the majority of the scarce Cu atom should incorporate onto the void of T-defect (as shown in Figure 1(f)) in polymeric carbon nitride.

To investigate the photocatalytic nitrogen fixation performance of the as-obtained samples, p-CN and Cu-CN were placed into N_2-saturated water and illuminated under visible light from a 300 W Xenon lamp with an UVIR cut-off filter (780 nm>λ>420 nm). The detailed experiment is described in the Methods section [48]. Considering that the defects, edges or terminal groups of the p-CN nanosheets contain a certain number of imino and amino groups, which may affect the chromogenic process of Nessler's agent, we first conducted the photocatalytic reaction in argon atmosphere as a reference to exclude such interference. As seen in Figure 2(a), no visible amount of ammonium was detected in argon atmosphere even under the irradiation, while remarkable ammonia production was observed in nitrogen atmosphere. No visual amount of ammonium was detected either both of the p-CN and Cu-CN in nitrogen atmosphere without the light irradiation (Figure S3(a)), which undoubtedly indicates that the produced NH_3 was derived from the nitrogen atmosphere and light irradiation rather than the intrinsic imino and amino groups of CN defects or edges. The total ammonia yield was evaluated by spectrophotometrically measuring the generated NH_3 with Nessler's reagent, and the results and producing rates are shown in Figure 2. As seen in Figure 2(a), the yield of ammonia in water containing 20% *v*/*v* ethanol reached 557 μmol g^{-1} after 3 h of photoillumination with an average ammonia-production rate of 186 μmol mol^{-1} h^{-1} by the Cu-CN catalyst, which is nearly 7 times higher than that by the pristine p-CN catalyst. The ion chromatography result of p-CN and Cu-CN for first hour's photocatalytic ammonia synthesis performance was displayed in Figure S3(b), in which the ammonia-production rate of Cu-CN and p-CN was 165 and 21.4 μmol g^{-1}, respectively, nearly close to the average spectrophotometrically results. And the quantum efficiency reached 1.01% under 420 nm monochromatic light (Figure S4). These results clearly verify that the introduction of single Cu atoms can significantly enhance the appearant performance of photocatalytic ammonia synthesis.

UV/Vis absorption spectra (Figure S5(a, b)) reveal the band gap of the prepared p-CN (2.50 eV) and Cu-CN (2.48 eV), which can be attributed to the introduction of metal ions into CN substrate. The valence band (VB) of both p-CN and Cu-CN is measured by XPS valence spectra, as shown in Figure S5(c). The p-CN displays a VB with the edge of the maximum energy at about 2.35 eV. That is to say, according to the optical absorption spectrum, the CB minimum would occur at about −0.15 eV. For the Cu-CN, the VB maximum energy up-shifts by 0.38 to 1.97 eV compared with that of p-CN. In this case, the CB minimum of Cu-CN up-shifts by 0.36 to −0.51 eV compared with that of p-CN (Figure S5(d)). The slightly narrowed width and up-shifted CB might result from the monodispersed copper ions, therefore the narrowed gap is beneficial for the absorption of

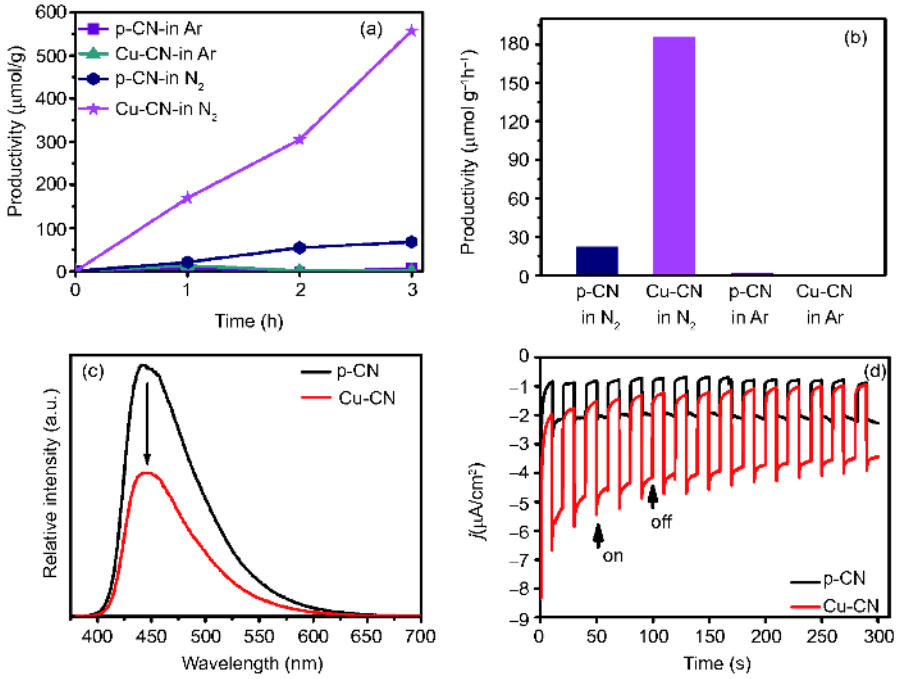

Figure 2 (a) Quantitative determination of NH_3 generated under visible light. (b) Photocatalytic ammonia-production rate under different atmospheres. (c) Photoluminescene spectra of p-CN and Cu-CN. (d) Photocurrent performance of p-CN and Cu-CN (−0.4 V vs. Ag/AgCl, pH=6.6) (color online).

the light therefore enhances the efficient genereation of excitons. The up-shifting of CB not only makes the photogenerated electrons more negative to involve the relative reaction but also promotes the transfer of photoexcited electrons to reactants, resulting in the inhibition of the electron-hole recombination. The strong photoluminescence quenching in the Cu-CN suggested that the recombination of photogenerated excitons was substantially suppressed (Figure 2(c)). An obvious enhanced photocurrent in the Cu-CN also implied that the efficient separation of the photoexcited charge carriers was promoted (Figure 2(d)).

The cause of such superior performance was worth *in-situ* investigating then we performed *in situ* FTIR spectroscopy under N_2 atmosphere and light irradiation to simulate the overall photocatalytic synthesis process, while monitoring the time-dependent changes of the functional groups on the catalyst surface [37]. As shown in Figure 3(a), several obvious bands arose with the extension of the irradiation time from 0 to 30 min in the Cu-CN sample, in contrast to the resulting spectrum of p-CN, in which no macroscopic change was observed (as shown in Figure S5), elucidating that the structural defects or edges, which contain abundant imino or amino groups, could not be the cause of such obvious changes. The selected areas in Figure 3(a) were amplified and shown in Figure 3(b, c). The band observed at 984 cm^{-1} and the band at 829 cm^{-1} were assigned to the ν(C–H) stretching mode outside the conjugated plane, which indicated the decomposition of adsorbed water and the weak interaction between the generated protons and the C atoms. The bands at 1553 and 1685 cm^{-1} were attributed to the σ(N–H) bending mode of the secondary amine or imine formed during light irradiation. These results suggested that the efficient formation of N–H bonds, and therefore the significant production of NH_3, occurred under N_2 atmosphere during light irradiation of Cu–CN. Therefore, we could reasonably illustrate the photocatalytic nitrogen reaction processes. The water adsorbed on the catalyst surface was decomposed to offer the protons, which would combine with the dinitrogen molecule and photoinduced excitons to initiate the following successive hydrogen addition reactions to produce ammonia.

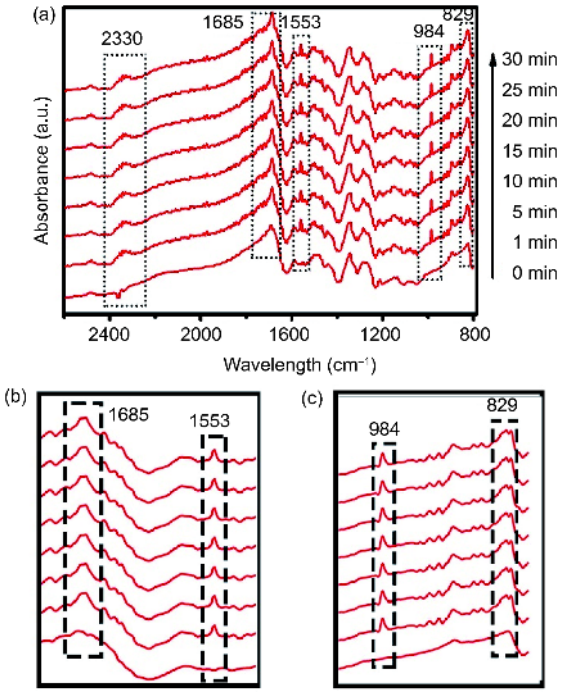

Figure 3 Photocatalytic synthesis of ammonia over the as-prepared Cu-CN. (a) *In situ* FTIR spectra recorded during the photocatalytic synthesis of ammonia over Cu-CN. (b) and (c) Amplified selected areas in Figure 3(a). The black dashed boxes indicate the changes during the procedure (color online).

To understand the origin of superior photocatalytic activity for ammonia synthesis, we performed ESR tests by dispersing the sample in ethanol, which can directly identify the active electrons in irradiated samples. Before irradiation, the characteristic broad peaks were assigned to the covalent character of the Cu(II)-ligand bond [49] inside Cu-CN, and the two compared samples only possessed minor peak shape similarities at approximately 3360 G (in Figure 4(a)), which was the signature of free electrons [50], origining from the abundant defects or edges amino group. When the light turned on, the ESR signals both in Cu-CN and p-CN at 3360 G were markedly enhanced (Figure 4(b)), but the intensity of this peak in Cu-CN was much higher than that in p-CN although the dispersions shared the same dispersed process and equivalent concentration, which suggested that a large concentration of extra free electrons were activated in Cu-CN under light irradiation. According to the physical configuration of CN we proposed above, the excitons usually originating from the trizaine/heptazine unit of the polymer, which containing abundant conjugated π electrons and terminal amino group. Through defect modification could we significantly enhance the relevant photocatalytic reaction [51]. In other words, the modification of structural unit in polymer do make a difference to the conjugated electron cloud. Then we focus on the structural unit of p-CN and Cu-CN. Apart from the approximated numerous terminal group, the edge N atom of the covalent ring was usually bound to two adjacent C atoms, leaving an unpaired electron to be conjugated into the π electron cloud. The lone-pair electrons of the N atoms possessed the last sp^2 hybridized orbital, which had a small angle to the absolute CN plane, resulting in the lone-pair electrons not being incorporated in the π electron cloud but rather stretching outside of the conjugated ring to become the potential adsorbing sites for exotic ions, such as protons and metal ions. The increase of the signal in p-CN generally originate from the activated terminal group and limited conjugated π electrons. While from the measured structural configuration and aforementioned simulation, in Cu-CN, one Cu atom was bound to

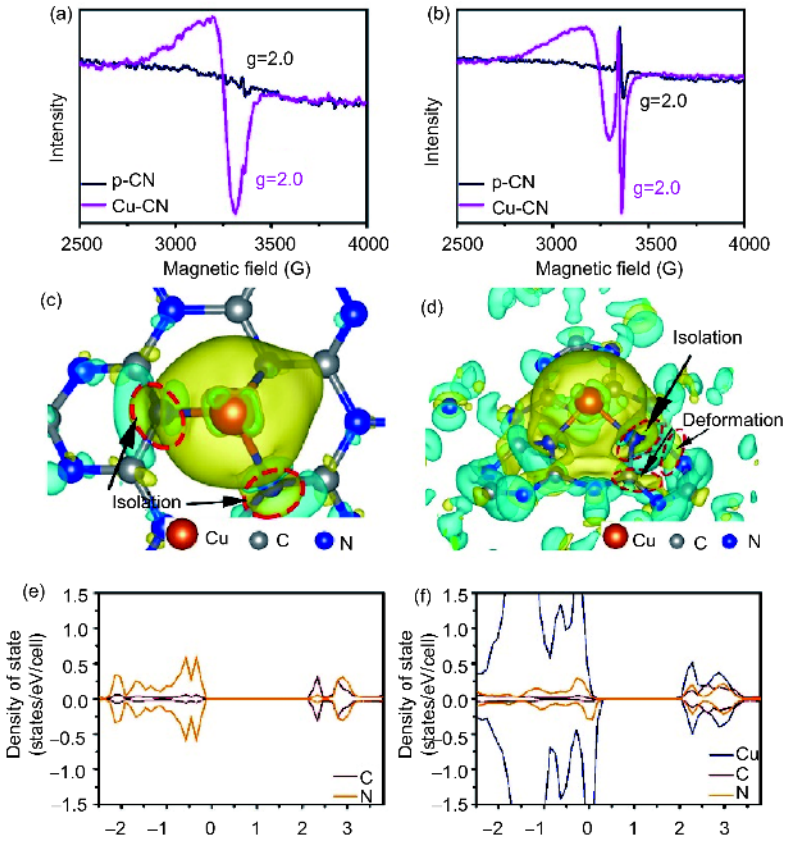

Figure 4 ESR of p-CN and Cu-CN (a) before and (b) during light irradiation. (c) Top view of the electron density distribution. (d) Side view of the electron density distribution. The yellow and green isosurfaces correspond to an increase in the number of electrons and the depletion zone, respectively. The isosurfaces are 0.003 e Å^{-3}. (e) Projected density of states of C and N atoms around the T-defect. (f) Projected density of states of Cu atoms, donor N atoms, and C atoms bound with the donor N atoms (color online).

three N atoms through lone-pair electrons to form a triangular pyramid configuration with three Cu-N bonds (Figure 1(f)), increasing the electronegativity and allowing the coordinated region to attract other electrons of the bonded N atoms. The spontaneous adsorption of the electron-rich dinitrogen molecule benefitted from the positively charged characteristic of Cu^{2+}, in contrast, the adsorption of N_2 molecule in p-CN seemed to be rather difficult because of the lack of appropriate adsorption sites (Table S4). The photoexcited electrons in copper(II) ion modified CN would transfer from the CN surface through Cu^{2+} ion to the antibond orbitals of the dinitrogen molecule during the photoexcitation, facilitating the cleavage of the strong triple bonds between two nitrogen atoms. On the other hand, the calculated different electron distribution, shown in Figure 4(c, d), vividly displays the efficient interactions between the Cu and N atoms amidst the catalyst surface. Strongly attracted by the Cu atom, the π conjugated electron cloud was deformed, and the single valence electron of the edge N atom was delocalized even isolated from the previous π electron cloud (green isosurfaces between the Cu atom and N atom represent the isolation effect). Those isolated valence electron fled from the constrainment of conjugated π electron cloud then contributed to the quantity of available active electron thus caused the additional increase in the signal we observed in the ESR signal, except the activated terminal group and limited π electrons already. For the C atoms adjacent to the coordinated N atoms, the electron number increased thus caused the carbon atoms negatively charged temporarily, attracting the protons spontaneously, which corresponding to the previous *in-situ* FTIR spectrum where resided the weak interaction of protons and C atoms. In addition, Figure 4(e, f) shows the calculated projected density of states (PDOS) for local T-defect in p-CN and Cu-CN, respectively. From Figure 4(e, f), we can clearly observe that the PDOS of the N atom of T-defect in Cu-CN was reduced by nearly 50% compared with that in p-CN due to copper coordination, which indicates an efficient decrease in the number of electrons in the π conjugated electron cloud upon introducing Cu atoms. Thus, the calculated PDOS also verifies the effective isolation of the single valence electron and the obvious deformation of the π conjugated electron cloud. The isolated valence electron can be easily activated and then promptly transfer through the interface of the metal ion to the dinitrogen molecule, therefore enhance the separation of the photoexcited electron-hole, inhibiting the recombination of

the photoexcited electron-hole. Such effect enlarges the quantity of available active electrons and promotes the transfer of the photo-generated electrons based on the manipulating the lone-pair electrons of defects in polymeric carbon nitride through single Cu atom coordination. According to the above experimental results and theoretical calculations analysis, it is reasonable to conclude that the single Cu atoms in T-defect of CN not only serve as the potential adsorption site for dinitrogen molecules but also significantly increase the quantity of activated electrons, which synergistically leads to the outstanding performance of photocatalytic ammonia synthesis.

4 Conclusions

In conclusion, the activity of the Cu-CN photocatalyst, represented here for the first time, towards the photoinduced synthesis of ammonia was 186 μmol g^{-1} h^{-1} under visible-light irradiation, and the quantum efficiency reached 1.01% under 420 nm monochromatic light. This catalyst would be a strong candidate for the superior performance of ammonia synthesis at the mild conditions with the scarce non-noble metal loading (Table S5, the bismuth based catalyst is intrinsically highly active for such relative reaction whereas our catalyst is basically aiming at manipulating the pristine catalytic activity of non-metal substrate). Through manipulating the lone-pair electrons in T-defect of polymeric carbon nitride with single Cu atom, not only do we provide a proof-of-concept that Cu-CN is highly active for ammonia synthesis but also shed scientific insight into the underlying mechanism of its significantly enhanced photocatalytic activity. Based on XAFS, *in situ* FTIR, ESR analysis and DFT calculations, the superior performance was found to arise from the additional large amount of active isolated π electrons and superior adsorption ability on the positively charged metal ions, which result from the coordination effect between lone-pair electrons of edge N atoms in p-CN with dispersed scarce single Cu atoms. This technique leads to the isolation of single valence electrons as well as the deformation of the conjugated π electron cloud. Considering that the lone-pair electrons and π electron cloud are typical characteristics of most conjugated polymers, it is reasonable to believe that this approach could be easily extended to other polymeric photocatalysts by carefully selecting the metal atom or even small molecule to induce the isolation of single valence electrons and the deformation of π electron cloud. Although there is still a long way to go to completely replace the well-established Haber-Bosch process by photocatalysis, the photocatalyst developed in this work undoubtedly offers a model to open a new avenues for ammonia synthesis under mild conditions. Furthermore, our approach also provides important insight into alternative pathways for many other photocatalytic reactions, such as water splitting and CO_2 reduction, due to the analogous main process of photoexcitation.

Acknowledgements This work was supported by the National Key R&D Program of China (2017YFA0207301), the National Natural Science Foundation of China (21622107, 11621063, U1532265), the Key Research Program of Frontier Sciences (QYZDY-SSW-SLH011), the Youth Innovation Promotion Association CAS (2016392), the Fundamental Research Funds of Central University (WK2340000075), and the Major Program of Development Foundation of Hefei Center for Physical Science and Technology (2017FXZY003). We thank Prof. J.H. Su from the University of Science and Technology of China for his helpful discussion of the ESR results. The computational center of USTC is acknowledged for computational support.

Conflict of interest The authors declare that they have no conflict of interest.

Supporting information The supporting information is available online at http://chem.scichina.com and http://link.springer.com/journal/11426. The supporting materials are published as submitted, without typesetting or editing. The responsibility for scientific accuracy and content remains entirely with the authors.

1 Chase MW. *NIST-JANAF Thermochemical Tables*. 4th ed. New York: American Chemical Society and American Institute of Physics, 1998
2 Hoffman BM, Lukoyanov D, Yang ZY, Dean DR, Seefeldt LC. *Chem Rev*, 2014, 114: 4041–4062
3 Rafiqul I, Weber C, Lehmann B, Voss A. *Energy*, 2005, 30: 2487–2504
4 Oshikiri T, Ueno K, Misawa H. *Angew Chem*, 2016, 128: 4010–4014
5 Rebreyend C, de Bruin B. *Angew Chem Int Ed*, 2015, 54: 42–44
6 Oshikiri T, Ueno K, Misawa H. *Angew Chem Int Ed*, 2014, 53: 9802–9805
7 Anderson JS, Rittle J, Peters JC. *Nature*, 2013, 501: 84–87
8 Fryzuk MD. *Science*, 2013, 340: 1530–1531
9 Macleod KC, Holland PL. *Nat Chem*, 2013, 5: 559–565
10 Li J, Li H, Zhan G, Zhang L. *Acc Chem Res*, 2017, 50: 112–121
11 Schrauzer GN, Guth TD. *J Am Chem Soc*, 1977, 99: 7189–7193
12 Liu J, Kelley MS, Wu W, Banerjee A, Douvalis AP, Wu J, Zhang Y, Schatz GC, Kanatzidis MG. *Proc Natl Acad Sci USA*, 2016, 113: 5530–5535
13 Zhu D, Zhang L, Ruther RE, Hamers RJ. *Nat Mater*, 2013, 12: 836–841
14 Lu X, Xu K, Tao S, Shao Z, Peng X, Bi W, Chen P, Ding H, Chu W, Wu C, Xie Y. *Chem Sci*, 2016, 7: 1462–1467
15 Li X, Bi W, Zhang L, Tao S, Chu W, Zhang Q, Luo Y, Wu C, Xie Y. *Adv Mater*, 2016, 28: 2427–2431
16 Ong WJ, Tan LL, Ng YH, Yong ST, Chai SP. *Chem Rev*, 2016, 116: 7159–7329
17 Yang P, Zhao J, Qiao W, Li L, Zhu Z. *Nanoscale*, 2015, 7: 18887–18890
18 Wang Y, Wang X, Antonietti M. *Angew Chem Int Ed*, 2012, 51: 68–89
19 Muetterties EL. *Science*, 1977, 196: 839–848
20 Moskovits M. *Acc Chem Res*, 1979, 12: 229–236
21 Marks TJ. *Acc Chem Res*, 1992, 25: 57–65
22 Quadrelli EA, Basset JM. *Coordin Chem Rev*, 2010, 254: 707–728
23 Copéret C, Chabanas M, Petroff Saint-Arroman R, Basset JM. *Angew Chem Int Ed*, 2003, 42: 156–181
24 Zhang Y, Thomas A, Antonietti M, Wang X. *J Am Chem Soc*, 2009, 131: 50–51
25 Xu K, Li X, Chen P, Zhou D, Wu C, Guo Y, Zhang L, Zhao J, Wu X, Xie Y. *Chem Sci*, 2015, 6: 283–287

26 Tyborski T, Merschjann C, Orthmann S, Yang F, Lux-Steiner MC, Schedel-Niedrig T. *J Phys-Condens Matter*, 2012, 24: 162201
27 Merschjann C, Tyborski T, Orthmann S, Yang F, Schwarzburg K, Lublow M, Lux-Steiner MC, Schedel-Niedrig T. *Phys Rev B*, 2013, 87: 205204
28 Wang H, Jiang S, Chen S, Li D, Zhang X, Shao W, Sun X, Xie J, Zhao Z, Zhang Q, Tian Y, Xie Y. *Adv Mater*, 2016, 28: 6940–6945
29 Iwase K, Yoshioka T, Nakanishi S, Hashimoto K, Kamiya K. *Angew Chem Int Ed*, 2015, 54: 11068–11072
30 Zhang G, Wang X. *J Catal*, 2013, 307: 246–253
31 Cao SW, Liu XF, Yuan YP, Zhang ZY, Fang J, Loo SCJ, Barber J, Sum TC, Xue C. *Phys Chem Chem Phys*, 2013, 15: 18363–18366
32 Caputo CA, Gross MA, Lau VW, Cavazza C, Lotsch BV, Reisner E. *Angew Chem Int Ed*, 2014, 53: 11538–11542
33 Liu P, Zhao Y, Qin R, Mo S, Chen G, Gu L, Chevrier DM, Zhang P, Guo Q, Zang D, Wu B, Fu G, Zheng N. *Science*, 2016, 352: 797–800
34 Zhu Y, Ramasse QM, Brorson M, Moses PG, Hansen LP, Kisielowski CF, Helveg S. *Angew Chem Int Ed*, 2014, 53: 10723–10727
35 Kistler JD, Chotigkrai N, Xu P, Enderle B, Praserthdam P, Chen CY, Browning ND, Gates BC. *Angew Chem Int Ed*, 2014, 53: 8904–8907
36 Hu P, Huang Z, Amghouz Z, Makkee M, Xu F, Kapteijn F, Dikhtiarenko A, Chen Y, Gu X, Tang X. *Angew Chem Int Ed*, 2014, 53: 3418–3421
37 Li H, Shang J, Ai Z, Zhang L. *J Am Chem Soc*, 2015, 137: 6393–6399
38 Kresse G, Hafner J. *Phys Rev B*, 1993, 47: 558–561
39 Blöchl PE. *Phys Rev B*, 1994, 50: 17953–17979
40 Kresse G, Furthmüller J. *Phys Rev B*, 1996, 54: 11169–11186
41 Kresse G, Joubert D. *Phys Rev B*, 1999, 59: 1758–1775
42 Perdew JP, Burke K, Ernzerhof M. *Phys Rev Lett*, 1996, 77: 3865–3868
43 Monkhorst HJ, Pack JD. *Phys Rev B*, 1976, 13: 5188–5192
44 Grimme S. *J Comput Chem*, 2006, 27: 1787–1799
45 Bucko T, Hafner J, Lebegue S, Angyan JG. *J Phys Chem A*, 2010, 114: 11814–11824
46 Ravel B, Newville M. *J Synchrotron Rad*, 2005, 12: 537–541
47 Zuo HW, Lu CH, Ren YR, Li Y, Zhang YF, Chen WK. *Acta Phys-Chim Sin*, 2016, 32: 1183–1190
48 Dong G, Ho W, Wang C. *J Mater Chem A*, 2015, 3: 23435–23441
49 Wu W, Zhan L, Fan W, Song J, Li X, Li Z, Wang R, Zhang J, Zheng J, Wu M, Zeng H. *Angew Chem Int Ed*, 2015, 54: 6540–6544
50 Easley WC, Weltner W Jr. *J Chem Phys*, 1970, 52: 197–205
51 Lau VWH, Moudrakovski I, Botari T, Weinberger S, Mesch MB, Duppel V, Senker J, Blum V, Lotsch BV. *Nat Commun*, 2016, 7: 12165